

# Measurement of main parameters of the $\psi(2S)$ resonance

V. V. Anashin<sup>a</sup>, V. M. Aulchenko<sup>a,b</sup>, E. M. Baldin<sup>a,b</sup>, A. K. Barladyan<sup>a</sup>, A. Yu. Barnyakov<sup>a</sup>, M. Yu. Barnyakov<sup>a</sup>, S. E. Baru<sup>a,b</sup>, I. Yu. Basok<sup>a</sup>, O. L. Beloborodova<sup>a,b</sup>, A. E. Blinov<sup>a</sup>, V. E. Blinov<sup>a,c</sup>, A. V. Bobrov<sup>a</sup>, V. S. Bobrovnikov<sup>a</sup>, A. V. Bogomyagkov<sup>a,b</sup>, A. E. Bondar<sup>a,b</sup>, A. R. Buzykaev<sup>a</sup>, S. I. Eidelman<sup>a,b</sup>, D. N. Grigoriev<sup>a</sup>, Yu. M. Glukhovchenko<sup>a</sup>, V. V. Gulevich<sup>a</sup>, D. V. Gusev<sup>a</sup>, S. E. Karnaev<sup>a</sup>, G. V. Karpov<sup>a</sup>, S. V. Karpov<sup>a</sup>, T. A. Kharlamova<sup>a,b</sup>, V. A. Kiselev<sup>a</sup>, V. V. Kolmogorov<sup>a</sup>, S. A. Kononov<sup>a,b</sup>, K. Yu. Kotov<sup>a</sup>, E. A. Kravchenko<sup>a,b</sup>, V. N. Kudryavtsev<sup>a</sup>, V. F. Kulikov<sup>a,b</sup>, G. Ya. Kurkin<sup>a,c</sup>, E. A. Kuper<sup>a,b</sup>, E. B. Levichev<sup>a,c</sup>, D. A. Maksimov<sup>a,b</sup>, V. M. Malyshev<sup>a</sup>, A. L. Maslennikov<sup>a</sup>, A. S. Medvedko<sup>a,b</sup>, O. I. Meshkov<sup>a,b</sup>, S. I. Mishnev<sup>a</sup>, I. I. Morozov<sup>a</sup>, N. Yu. Muchnoi<sup>a</sup>, V. V. Neufeld<sup>a</sup>, S. A. Nikitin<sup>a</sup>, I. B. Nikolaev<sup>a,b</sup>, I. N. Okunev<sup>a</sup>, A. P. Onuchin<sup>a,c</sup>, S. B. Oreshkin<sup>a</sup>, I. O. Orlov<sup>a,b</sup>, A. A. Osipov<sup>a</sup>, S. V. Peleganchuk<sup>a</sup>, S. G. Pivovarov<sup>a,c</sup>, P. A. Piminov<sup>a</sup>, V. V. Petrov<sup>a</sup>, A. O. Poluektov<sup>a</sup>, V. G. Prisekin<sup>a</sup>, A. A. Ruban<sup>a</sup>, V. K. Sandyrev<sup>a</sup>, G. A. Savinov<sup>a</sup>, A. G. Shamov<sup>a,\*</sup>, D. N. Shatilov<sup>a</sup>, B. A. Shwartz<sup>a,b</sup>, E. A. Simonov<sup>a</sup>, S. V. Sinyatkin<sup>a</sup>, A. N. Skrinsky<sup>a</sup>, V. V. Smaluk<sup>a</sup>, A. V. Sokolov<sup>a</sup>, A. M. Sukharev<sup>a</sup>, E. V. Starostina<sup>a,b</sup>, A. A. Talyshev<sup>a,b</sup>, V. A. Tayursky<sup>a,b</sup>, V. I. Telnov<sup>a,b</sup>, Yu. A. Tikhonov<sup>a,b</sup>, K. Yu. Todyshev<sup>a,b,\*</sup>, G. M. Tumaikin<sup>a</sup>, Yu. V. Usov<sup>a</sup>, A. I. Vorobiov<sup>a</sup>, A. N. Yushkov<sup>a</sup>, V. N. Zhilich<sup>a</sup>, V. V. Zhulanov<sup>a,b</sup>, A. N. Zhuravlev<sup>a,b</sup>

<sup>a</sup>*Budker Institute of Nuclear Physics, Russian Acad. Sci. Sibirian Div., 630090, Novosibirsk, Russia*

<sup>b</sup>*Novosibirsk State University, 630090, Novosibirsk, Russia*

<sup>c</sup>*Novosibirsk State Technical University, 630092, Novosibirsk, Russia*

## Abstract

A high-precision determination of the main parameters of the  $\psi(2S)$  resonance has been performed with the KEDR detector at the VEPP-4M  $e^+e^-$  collider in three scans of the  $\psi(2S)$ – $\psi(3770)$  energy range. Fitting the energy dependence of the multihadron cross section in the vicinity of the  $\psi(2S)$  we obtained the mass value

$$M = 3686.114 \pm 0.007 \pm 0.011^{+0.002}_{-0.012} \text{ MeV}$$

and the product of the electron partial width by the branching fraction into hadrons

$$\Gamma_{ee} \times \mathcal{B}_h = 2.233 \pm 0.015 \pm 0.037 \pm 0.020 \text{ keV}.$$

The third error quoted is an estimate of the model dependence of the result due to assumptions on the interference effects in the cross section of the single-photon  $e^+e^-$  annihilation to hadrons explicitly considered in this work. Implicitly, the same assumptions were employed to obtain the charmonium leptonic width and the absolute branching fractions in many experiments.

Using the result presented and the world average values of the electron and hadron branching fractions, one obtains the electron partial width and the total width of the  $\psi(2S)$ :

$$\begin{aligned} \Gamma_{ee} &= 2.282 \pm 0.015 \pm 0.038 \pm 0.021 \text{ keV}, \\ \Gamma &= 296 \pm 2 \pm 8 \pm 3 \text{ keV}. \end{aligned}$$

These results are consistent with and more than two times more precise than any of the previous experiments.

## 1. Introduction

More than thirty six years passed since the discovery of  $J/\psi$ , but studies of charmonium states still raise new questions. Recent progress in charmonium physics requires an improvement of the accuracy of the parameters of charmonium states [1]. This Letter describes a measurement of the  $\psi(2S)$  meson parameters in the KEDR experiment performed during energy scans from 3.67 to 3.92 GeV at the VEPP-4M  $e^+e^-$  collider.

For a precision experiment it is essential to state explicitly what quantities are measured and how they can be compared with results of theoretical studies, therefore we discuss a definition of the  $\psi(2S)$  parameters just after a brief description of the experiment. The importance of the question has grown since the appearance of the work [2] in which the BES collaboration used an original approach to the determination of the  $J^{PC} = 1^{--}$  resonance parameters. Its further modification has been used in Refs. [3, 4, 5].

\*Corresponding authors, e-mails:  
shamov@inp.nsk.su, todyshev@inp.nsk.su

## 2. VEPP-4M collider and KEDR detector

VEPP-4M is an  $e^+e^-$  collider [6] designed for high-energy physics experiments in the center-of-mass (c.m.) energy range from 2 to 12 GeV. The peak luminosity in the  $2 \times 2$  bunches operation mode is about  $2 \times 10^{30} \text{ cm}^{-2} \text{ s}^{-1}$  in the vicinity of  $\psi(2S)$ . Having a modest luminosity, VEPP-4M is well equipped for high-precision measurements of beam energy [7]. The instantaneous value of the beam energy can be calibrated using the resonant depolarization method (RDM) [8, 9] with the relative accuracy of about  $10^{-6}$ . The results of RDM calibrations must be interpolated to determine the energy during data taking and the interpolation accuracy of about 10 keV can be reached [10]. Continuous energy monitoring is performed using the infrared light Compton backscattering [11] with the accuracy of the method  $\sim 60 \text{ keV}$ .

The KEDR detector [12] (Fig. 1) comprises the vertex detector (VD), drift chamber (DC), time-of-flight (TOF) system of scintillation counters, particle identification system based on the aerogel Cherenkov counters, EM calorimeter (liquid krypton in the barrel part and CsI crystals in the endcaps), superconducting magnet system and muon system inside the magnet yoke. The superconducting solenoid provides a longitudinal magnetic field of 0.6 T. The detector is equipped with a scattered electron tagging system for two-photon studies and some applications. The on-line luminosity measurement is provided by two independent single bremsstrahlung monitors. The trigger consists of two hardware levels: the primary trigger (PT) and the secondary one (ST) [13]. The PT operates using signals from the TOF counters and fast signals from the CsI and LKr calorimeters, whereas the ST uses the normally shaped calorimeter signals and the information from VD, DC and TOF system. After the readout, a software selection of events is performed using simplest event characteristics, in particular, the number of hits in VD. The upper limit on the number of VD tubes hit is very effective for the machine background suppression.

### 3. Data sample

In 2004 two scans of the  $\psi(2S)$ – $\psi(3770)$  energy range were carried out with an integrated luminosity of about  $0.7 \text{ pb}^{-1}$ . In 2006 the regions of  $\psi(2S)$  and  $\psi(3770)$  mesons were scanned once again with an integrated luminosity of  $\approx 1.9 \text{ pb}^{-1}$ . The combined data sample corresponds to  $1.6 \cdot 10^5 \psi(2S)$  produced. The data acquisition scenario for  $\psi(2S)$  was similar to that described in Ref. [10]. The accuracy of the energy interpolation between the RDM calibrations varied from 10 to 30 keV during the whole experiment. Our final results on the  $\psi(3770)$  parameters are presented in the next letter of this volume.

### 4. On definition of $J^{PC} = 1^{--}$ resonance parameters

A resonance with the quantum numbers  $J^{PC} = 1^{--}$  can be treated in some cases not as an unstable particle but just as a vacuum polarization phenomenon. Sometimes this causes confusion in the data analysis as was noted in Ref. [14]. To avoid

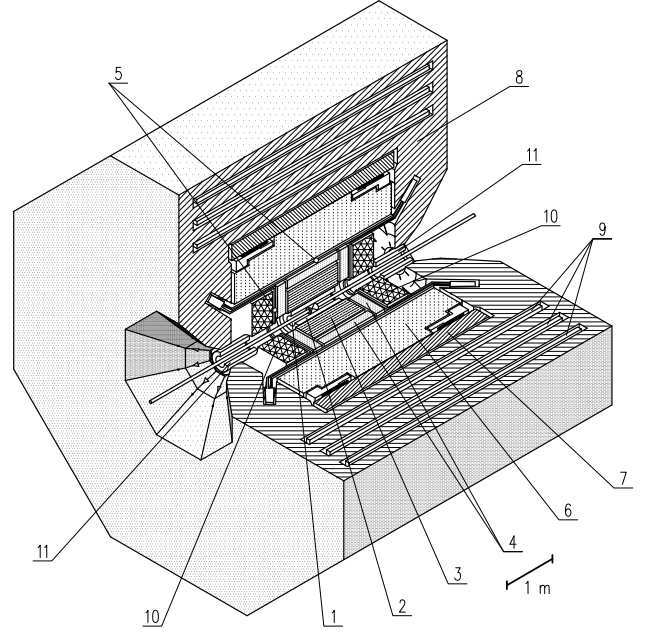


Figure 1: 1 – Vacuum chamber, 2 – Vertex detector, 3 – Drift chamber, 4 – Threshold aerogel counters, 5 – ToF-counters, 6 – Liquid krypton calorimeter, 7 – Superconducting solenoid, 8 – Magnet yoke, 9 – Muon tubes, 10 – CsI calorimeter, 11 – Compensating superconducting coils

confusion, “bare” and “dressed” or “physical” parameters of a resonance must be clearly distinguished. The former do not include QED corrections and are used in many theoretical studies, the latter include some of them (in particular, the vacuum polarization) and are published as results of almost all experimental papers.

The physical parameters correspond to the interpretation of a  $1^{--}$  resonance as a particle described with a Breit-Wigner amplitude representing its appearance in all orders of the QED perturbations, which is absolutely natural for the strong production of a resonance, e.g., in the process  $e^+e^- \rightarrow \psi(2S) \rightarrow p\bar{p}$ , this amplitude interferes with the pure QED amplitude of the  $e^+e^- \rightarrow p\bar{p}$  transition. As shown below, such an approach allows one to avoid the numerical integration in the calculation of radiative corrections.

Let us demonstrate the relation between the bare and physical parameters. According to Ref. [15], the cross section of the single-photon annihilation can be written in the form

$$\sigma(s) = \int dx \frac{\sigma_0((1-x)s)}{|1 - \Pi((1-x)s)|^2} \mathcal{F}(s, x), \quad (1)$$

where  $s$  is the c.m. energy squared,  $\mathcal{F}(s, x)$  is the radiative correction function,  $\Pi(s)$  represents the vacuum polarization operator and  $\sigma_0(s)$  is the Born cross section of the process. One has  $\Pi = \Pi_0 + \Pi_R$  with the nonresonant  $\Pi_0 = \Pi_{ee} + \Pi_{\mu\mu} + \Pi_{\tau\tau} + \Pi_{\text{hadr}}$  and the resonant

$$\Pi_R(s) = \frac{3\Gamma_{ee}^{(0)}}{\alpha} \frac{s}{M_0} \frac{1}{s - M_0^2 + iM_0\Gamma_0}, \quad (2)$$

where  $\alpha$  is the fine structure constant,  $M_0$ ,  $\Gamma_0$  and  $\Gamma_{ee}^{(0)}$  are the “bare” resonance mass, total and electron widths, respectively. Eq. (2) slightly differs from the expression used in Refs. [16, 17]. It corresponds to the simplest resonance cross section parameterization

$$\sigma_R(s) = -\frac{4\alpha}{s} \text{Im} \Pi_R(s) = \frac{12\pi\Gamma_{ee}^{(0)}\Gamma_0}{(s - M_0^2)^2 + M_0^2\Gamma_0^2}. \quad (3)$$

For the muon pair production the Born cross section at  $s \gg 4m_\mu^2$  ( $m_\mu$  is the muon mass) is just

$$\sigma_0^{\mu\mu}(s) = \frac{4\pi\alpha^2}{3s}, \quad (4)$$

thus the resonance behaviour of the cross section is, in this approach, entirely due to the vacuum polarization, which implicitly describes the muonic decay of a resonance. Eqs. (1), (2) and (4) give the dimuon cross section without separation into the continuum, resonant and interference parts. To obtain the contribution of the resonance, the continuum part must be subtracted from the amplitude. It can be done with the identity

$$\frac{1}{1 - \Pi_0 - \Pi_R(s)} \equiv \frac{1}{1 - \Pi_0} + \frac{1}{(1 - \Pi_0)^2} \frac{3\Gamma_{ee}^{(0)}}{\alpha} \frac{s}{M_0} \frac{1}{s - \tilde{M}^2 + i\tilde{M}\tilde{\Gamma}} \quad (5)$$

Two terms in the right-hand side correspond to the continuum amplitude and the resonant one, respectively. The second power of the vacuum polarization factor  $1/(1 - \Pi_0)$  in the latter can be interpreted as the presence of two photons, one at a resonance production and the other in its decay. In the resonant amplitude both  $\tilde{M}$  and  $\tilde{\Gamma}$  depend on  $s$

$$\begin{aligned} \tilde{M}^2 &= M_0^2 + \frac{3\Gamma_{ee}^{(0)}}{\alpha} \frac{s}{M_0} \text{Re} \frac{1}{1 - \Pi_0}, \\ \tilde{M}\tilde{\Gamma} &= M_0\Gamma_0 - \frac{3\Gamma_{ee}^{(0)}}{\alpha} \frac{s}{M_0} \text{Im} \frac{1}{1 - \Pi_0}. \end{aligned} \quad (6)$$

In the vicinity of a narrow resonance this dependence is negligible, thus the resonant contribution can be described with a simple Breit-Wigner amplitude containing the physical parameters  $M \approx \tilde{M}(M_0^2)$  and  $\Gamma \approx \tilde{\Gamma}(M_0^2)$ .

To obtain the dimuon cross section one has to multiply the absolute value squared of the right-hand side of Eq. (5) by the Born cross section (4). The resonant part of the cross section is proportional to  $\Gamma_{ee}^{(0)}$  squared which appears instead of  $\Gamma_{ee}^{(0)}\Gamma_{\mu\mu}^{(0)}$  due to the lepton universality in QED. The factor  $1/(1 - \Pi_0)^2$  in front of the resonance amplitude converts the square of the bare  $\Gamma_{ee}^{(0)}$  to the square of the physical partial width

$$\Gamma_{ee} = \frac{\Gamma_{ee}^{(0)}}{|1 - \Pi_0|^2} \quad (7)$$

recommended to use by Particle Data Group since the work [18] appeared.

For electromagnetic decays of a resonance to hadrons, the only difference with the dimuon case is the factor  $R$  in the cross

section, where  $R$  is the hadron-to-muon cross section ratio off the resonance peak. For a strong decay with the partial width  $\Gamma_0^{(s)}$  the Born cross section is

$$\sigma_0^{(s)}(s) = \frac{12\pi\Gamma_{ee}^{(0)}\Gamma_0^{(s)}}{(s - M_0^2)^2 + M_0^2\Gamma_0^2}. \quad (8)$$

In this case the identity (5) is not required, the direct substitution of (2) and (8) in (1) leads to the same definition of the physical mass, total width and leptonic width. The equivalent definition of the physical mass in the hadronic channel is given in Ref. [19]. The physical value of the partial width  $\Gamma^{(s)}$  is identical to the bare one  $\Gamma_0^{(s)}$ .

We would like to emphasize that the experimental values of a  $1^{--}$  resonance mass, total or leptonic width can not be compared with the immediate results of potential models or used to fit parameters of a potential without either “undressing” of the experimental values or “dressing” of the potential model results with Eqs. (6) and (7). The differences between dressed and bare masses are about 1.2 and 0.5 MeV for the  $J/\psi$  and  $\psi(2S)$ , respectively. The corresponding differences for the total widths are about 23 and 10 keV ( $\text{Im} \Pi_0 \approx -\alpha(R+2)/3$  with the  $R$  ratio about 2.2).

Unlike the works [2, 3], we consistently use the physical parameters and treat equally strong and electromagnetic decays of the  $\psi(2S)$ . The difference in the approaches is discussed in more detail in Section 5.3. It is worth noting that we do not suggest any new approach, but just follow the one employed in most measurements of heavy quarkonium parameters though, as far as we know, its relation to Eq. (1) in the hadronic and leptonic channels was not rigorously considered until recently.

## 5. Cross section calculation

The cross section formulae given below in this section contain the  $\psi(2S)$  total width  $\Gamma$  and the electronic width  $\Gamma_{ee}$ , the determination of which are the goal of our analysis. We fix these parameters in the cross section fit, but use the iteration procedure to obtain the final results. The values of the  $\psi(2S)$  electron and hadron branching fractions, required to recalculate  $\Gamma_{ee} \times \mathcal{B}_h$  to  $\Gamma_{ee}$  and  $\Gamma$ , are fixed at the world averages. The systematic uncertainties due to such an approach are discussed in Section 7.4.

### 5.1. Multihadron cross section

Below we present the results of the paper [20] published soon after  $J/\psi$  discovery in the updated interpretation. Some details of the analytical calculations and numerical checks can be found in Ref. [21].

Using the physical values of the parameters, for strong decays of  $\psi(2S)$  one reduces Eq. (1) to

$$\begin{aligned} \sigma_{\psi(2S)}^{RC}(W) &= \int \frac{12\pi\Gamma_{ee}\Gamma_h^{(s)}}{(W^2(1-x) - M^2)^2 + M^2\Gamma^2} \\ &\quad \times \mathcal{F}(x, W^2) dx, \end{aligned} \quad (9)$$

where  $W = \sqrt{s}$  is the total collision energy,  $\Gamma$ ,  $\Gamma_{ee}$  and  $\Gamma_h^{(s)}$  are the total and partial widths of the  $\psi(2S)$  meson, and  $M$  is its mass.

Taking into account the resonance-continuum interference and performing the integration over  $x$  with a simplified version of  $\mathcal{F}(x, s)$  one obtains

$$\begin{aligned} \sigma_{\psi(2S)}^{RC}(W) = & \frac{12\pi}{W^2} \left\{ \left(1 + \delta_{sf}\right) \left[ \frac{\Gamma_{ee}\tilde{\Gamma}_h}{\Gamma M} \text{Im} f(W) \right. \right. \\ & - \left. \frac{2\alpha\sqrt{R\Gamma_{ee}\tilde{\Gamma}_h}}{3W} \lambda \text{Re} \frac{f^*(W)}{1-\Pi_0} \right] \\ & - \frac{\beta\Gamma_{ee}\tilde{\Gamma}_h}{2\Gamma M} \left[ \left(1 + \frac{M^2}{W^2}\right) \arctan \frac{\Gamma W^2}{M(M^2 - W^2 + \Gamma^2)} \right. \\ & \left. \left. - \frac{\Gamma M}{2W^2} \ln \frac{\left(\frac{M^2}{W^2}\right)^2 + \left(\frac{\Gamma M}{W^2}\right)^2}{\left(1 - \frac{M^2}{W^2}\right)^2 + \left(\frac{\Gamma M}{W^2}\right)^2} \right] \right\}, \end{aligned} \quad (10)$$

where  $\Pi_0$  is the vacuum polarization operator with the  $\psi(2S)$  contribution excluded. The  $\tilde{\Gamma}_h$  parameter includes both strong and electromagnetic decays and some contribution of interference effects which is discussed in the next subsection.

The first square bracket in Eq. (10) corresponds to radiation of soft photons, while the second one represents hard photon corrections. The  $\lambda$  parameter introduced in Ref. [20] characterizes the strength of the interference effect in the multihadron cross section and equals 1 for the dimuon cross section.

The correction  $\delta_{sf}$  follows from the structure function approach of Ref. [15]:

$$\delta_{sf} = \frac{3}{4}\beta + \frac{\alpha}{\pi} \left( \frac{\pi^2}{3} - \frac{1}{2} \right) + \beta^2 \left( \frac{37}{96} - \frac{\pi^2}{12} - \frac{1}{36} \ln \frac{W}{m_e} \right), \quad (11)$$

$$\beta = \frac{4\alpha}{\pi} \left( \ln \frac{W}{m_e} - \frac{1}{2} \right), \quad (12)$$

$m_e$  is the electron mass and the function  $f$  is defined with

$$f(W) = \frac{\pi\beta}{\sin\pi\beta} \left( \frac{W^2}{M^2 - W^2 - iM\Gamma} \right)^{1-\beta}. \quad (13)$$

The presentation of the soft photon integrals in form of the real and imaginary parts of the function  $f$  is more transparent than that of Ref. [22].

Despite a simplification of  $\mathcal{F}(x, s)$ , not too far from the  $\psi(2S)$  peak the resonant part of Eq. (10) reproduces the results obtained by the numerical integration of the complete formula with an accuracy better than 0.1%.

The resonant part of Eq. (10) is proportional to the  $\Gamma_{ee}\tilde{\Gamma}_h/\Gamma$  combination which is a product of the partial width and the branching fraction:  $\Gamma_{ee} \times \tilde{\mathcal{B}}_h = \tilde{\Gamma}_h \times \mathcal{B}_{ee}$ . Since our final result is  $\Gamma_{ee} \times \mathcal{B}_h$ , let us consider the relation of  $\tilde{\Gamma}_h$  with the true  $\Gamma_h$ , which is a sum of hadronic partial widths.

## 5.2. Interference effects in total multihadron cross section

Considering charmonium decays at the parton level, one deals with the gluonic  $\psi \rightarrow gg(g/\gamma)$  and electromagnetic  $\psi \rightarrow$

$\gamma^* \rightarrow q\bar{q}$  modes. Treating quarks and gluons as final decay products, one obtains that gluonic modes do not interfere with the continuum  $e^+e^- \rightarrow \gamma^* \rightarrow q\bar{q}$  process while those of electromagnetic origin do with the interference phase equal to that of the dimuon decay. In this case  $\tilde{\Gamma}_h$  does not differ from a sum of the hadronic partial widths  $\Gamma_h = \Gamma_{gg(g\gamma)} + \Gamma_{q\bar{q}}$  with  $\Gamma_{q\bar{q}} = R\Gamma_{ee}$  and

$$\lambda = \sqrt{\frac{R\mathcal{B}_{ee}}{\mathcal{B}_h}}, \quad (14)$$

where  $\mathcal{B}_{ee}$  and  $\mathcal{B}_h$  denote the electron and hadron branching fractions, respectively. The real situation is much more complicated.

For an exclusive hadronic mode  $m$  at a given point in the decay product phase space  $\Theta$  the amplitude  $e^+e^- \rightarrow m$  can be written as

$$\begin{aligned} A_m(\Theta) = & \sqrt{\frac{12\pi}{W^2}} \left( \frac{\alpha}{3} \frac{a_m(\Theta) \sqrt{R_m}}{1-\Pi_0} - \right. \\ & \left. \frac{a_m(\Theta) M \sqrt{R_m\Gamma_{ee}^2} + a_m^{(s)}(\Theta) e^{i\phi_m} M \sqrt{\Gamma_{ee}\Gamma_m^{(s)}}}{M^2 - W^2 - iM\Gamma} \right), \end{aligned} \quad (15)$$

where  $R_m$  is the mode contribution to  $R$ ,  $\Gamma_m^{(s)}$  represents the contribution of the strong interaction to the partial width and  $\phi_m$  is its phase relative to the electromagnetic contribution  $\Gamma_m^{(\gamma)} = R_m\Gamma_{ee}$ , the real functions  $a$  are normalized with  $\int a_m^2(\Theta) d\Theta = 1$ . In general, the phase  $\phi_m$  depends on  $\Theta$ . The numerator of the last term of Eq.(15) is proportional to the decay amplitude, the partial width is

$$\Gamma_m = R_m\Gamma_{ee} + \Gamma_m^{(s)} + 2\sqrt{R_m\Gamma_{ee}\Gamma_m^{(s)}} \langle \cos \phi_m \rangle_{\Theta}, \quad (16)$$

where the angle brackets denote averaging over the product phase space:  $\langle x(\Theta) \rangle_{\Theta} \equiv \int a(\Theta) x(\Theta) d\Theta$ . To obtain the exclusive mode cross section, the following replacement must be done in the expression (10):

$$\begin{aligned} \Gamma_m & \rightarrow \tilde{\Gamma}_h, \quad 1 \rightarrow \lambda, \quad R_m \rightarrow R, \\ \text{Re} \left( \sqrt{R_m\mathcal{B}_{ee}} + \langle e^{-i\phi_m} \rangle_{\Theta} \sqrt{\frac{\Gamma_m^{(s)}}{\Gamma_m}} \right) \frac{f^*(W)}{1-\Pi_0} & \rightarrow \text{Re} \frac{f^*(W)}{1-\Pi_0}, \end{aligned} \quad (17)$$

where the latter replacement follows from comparison of the interference term corresponding to Eq. (15) and that of Eq. (10). Performing them and summing over all hadronic modes one obtains the expressions for  $\tilde{\Gamma}_h$  and  $\lambda$ :

$$\begin{aligned} \tilde{\Gamma}_h & = \Gamma_h \times \\ & \left( 1 + \frac{2\alpha}{3(1-\text{Re}\Pi_0)\mathcal{B}_h} \sqrt{\frac{R}{\mathcal{B}_{ee}}} \sum_m \sqrt{b_m\mathcal{B}_m^{(s)}} \langle \sin \phi_m \rangle_{\Theta} \right) \end{aligned} \quad (18)$$

(here  $\Gamma_h = \sum_m \Gamma_m$ ,  $\text{Im}\Pi_0$  is neglected),

$$\lambda = \sqrt{\frac{R\mathcal{B}_{ee}}{\mathcal{B}_h}} + \sqrt{\frac{1}{\mathcal{B}_h}} \sum_m \sqrt{b_m\mathcal{B}_m^{(s)}} \langle \cos \phi_m \rangle_{\Theta}, \quad (19)$$

where  $b_m = R_m/R$  is a branching fraction of the continuum process and  $\mathcal{B}_m^{(s)} = \Gamma_m^{(s)}/\Gamma$ . Below, the sums containing  $\langle \sin \phi_m \rangle_\Theta$  and  $\langle \cos \phi_m \rangle_\Theta$  are referred to as  $\Sigma_{\sin}$  and  $\Sigma_{\cos}$ , respectively. The parton level results are reproduced by Eq.(18) and (19) if  $\Sigma_{\sin}$  and  $\Sigma_{\cos}$  can be neglected. For a hypothetical heavy charmonium decaying to light hadrons, both the values of  $\langle \cos \phi_m \rangle_\Theta$  and  $\langle \sin \phi_m \rangle_\Theta$  averaged over the product phase space tend to zero due to the different configuration of jets in electromagnetic and strong decays. For the real  $J/\psi$  and  $\psi(2S)$  one has to rely on the absence of the phase correlations in different decays. For the quasi-two-body decays such correlations are expected (Ref. [23] and references therein) but their branching fractions are small [24].

If the sum  $\Sigma_{\sin}$  is not negligible, the method of the resonant cross section determination employed in this and many other experiments becomes inaccurate and ambiguous because of the well-known ambiguity in the partial width determination which takes place for each individual mode. Indeed, a fit of the mode cross section  $\sigma_m$  gives the values of  $\tilde{\Gamma}_m$  and  $\cos \phi_m$  but leaves unknown a sign of  $\sin \phi_m$  required to obtain  $\Gamma_m$ .

Equating all  $\langle \sin \phi_m \rangle_\Theta$  in Eq. (18) to unity, one sets an upper limit on the inaccuracy of the hadronic partial width  $\Delta\Gamma_h$  and the resonant cross section at the peak  $\Delta\sigma_h^{\text{res}}(W_{\text{peak}})$  used for the determination of the branching fractions:

$$\frac{\Delta\sigma_h^{\text{res}}(W_{\text{peak}})}{\sigma_h^{\text{res}}(W_{\text{peak}})} \approx \frac{\Delta\Gamma_h}{\Gamma_h} \lesssim \frac{2\alpha}{3\mathcal{B}_h} \sqrt{\frac{R}{\mathcal{B}_{ee}}} \sum_m \sqrt{b_m \mathcal{B}_m^{(s)}}. \quad (20)$$

For  $\psi(2S)$  the sum in the right part  $\lesssim 1 - \mathcal{B}_{J/\psi+X}$ , thus Eq. (20) gives about 4%. A better estimate employing the  $\lambda$  value obtained with the cross section fit is discussed in Section 8. Until this section we omit the tilde mark wherever possible, thus  $\Gamma_h$  and  $\mathcal{B}_h$  should be read as  $\tilde{\Gamma}_h$  and  $\tilde{\mathcal{B}}_h$ .

Eqs. (18) and (19) show that the correct account of interference effects is essential for a determination of the  $\psi(3770)$  parameters due to its small value of  $\mathcal{B}_{ee}$  and large branching fraction to  $D$  mesons, nevertheless, it was ignored in most of published analyses. The interference effect is crucial for a determination of the non- $D\bar{D}$  decay fraction of  $\psi(3770)$  as was emphasized in Ref. [25].

### 5.3. Observed multihadron cross section

The multihadron cross section observed experimentally in the vicinity of  $\psi(2S)$  can be parameterized as follows:

$$\sigma_{\psi(2S)}^{\text{obs}}(W) = \varepsilon_{\psi(2S)} \int \sigma_{\psi(2S)}^{\text{RC}}(W') G(W, W') dW' + \varepsilon_{\tau\tau} \sigma_{\text{cont}}^{\tau\tau}(W) + \sigma_{\text{cont}}(W). \quad (21)$$

Here  $\varepsilon_{\psi(2S)}$  and  $\varepsilon_{\tau\tau}$  are the detection efficiencies and their dependence on  $W$  can be neglected. The continuum  $\tau^+\tau^-$  cross section  $\sigma_{\tau\tau}$  is included according to Ref. [26] to extend the validity of (21) beyond the  $\psi(2S)$ - $\psi(3770)$  region.

For the  $\psi(2S)$  cross section (10) includes the  $\tau$  contribution and the  $\lambda$  parameter is modified properly:

$$\lambda_{h+\tau} \approx \sqrt{\frac{R\mathcal{B}_{ee}}{\mathcal{B}_h}} + \frac{\varepsilon_{\tau\tau}}{\varepsilon_{\psi(2S)}} \sqrt{\frac{R_\tau \mathcal{B}_{\tau\tau}}{R \mathcal{B}_h}} \quad (22)$$

with  $R_\tau = \sigma_{\tau^+\tau^-}/\sigma_{\mu^+\mu^-} \approx 0.39$ . The reduction of  $\tau^+\tau^-$  detection efficiency of about 0.3 compared to the multihadron one is accounted explicitly.

In Eq. (21) this cross section is folded with the distribution over the total collision energy which is assumed to be quasi-Gaussian with an energy spread  $\sigma_W$ :

$$G(W, W') = \frac{g(W-W')}{\sqrt{2\pi}\sigma_W} \exp\left(-\frac{(W-W')^2}{2\sigma_W^2}\right). \quad (23)$$

The preexponential factor can be written as

$$g(\Delta) = \frac{1 + a\Delta + b\Delta^2}{1 + b\sigma_W^2}. \quad (24)$$

It is due to various accelerator effects such as the  $\beta$ -function chromaticity. We fix  $a = b = 0$  in our fit and consider the corresponding systematic errors in the  $\Gamma_{ee} \times \mathcal{B}_h$  product in Section 7.3. The presence of this factor and other accelerator- and detector-related effects yield too large systematic uncertainties when the total width parameter  $\Gamma$  is left floating in the fit at  $\sigma_W \gtrsim 5 \times \Gamma/2$ .

Since the interference effect is included in  $\sigma_{\psi(2S)}^{\text{RC}}$ , the continuum cross section is a smooth function, which with the sufficient accuracy can be parameterized with

$$\sigma_{\text{cont}}(W) = \sigma_0 \left(\frac{W_0}{W}\right)^2, \quad (25)$$

where  $\sigma_0$  is the value of the background cross section at a fixed energy  $W_0$  below the  $\psi(2S)$  peak.

In contrast with the commonly used interpretation of the cross section as a sum of the resonant, continuum and interference parts employed, in particular, in Ref. [2], in the works [3, 4, 5] it is interpreted as a sum of the two parts only: the cross section of the resonance and the ‘‘nonresonant’’ one. The latter is calculated using the full vacuum polarization operator  $\Pi_0 + \Pi_{\psi(2S)}$  (Eq. (10) of Ref. [3]). The two approaches are equivalent provided that the bare parameters enter the  $\Pi_{\psi(2S)}$  and the electromagnetic contribution is excluded from the cross section of the resonance (Eq. (3) of Ref. [3]). The full vacuum polarization operator describes not only the interference, but the electromagnetic decays as well. If it is not done, the electron width extracted from the cross section fit would have a negative bias of about  $R \cdot \mathcal{B}_{ee}/\mathcal{B}_h \approx 0.018$ .

### 5.4. Observed $e^+e^-$ cross section

Bhabha scattering events detected in the calorimeter were employed for luminosity measurements (see Section 6.3 for more detail). For the large angle Bhabha scattering the contribution of  $\psi(2S)$  decays is not negligible. The differential  $e^+e^-$  cross section can be calculated with

$$\left(\frac{d\sigma}{d\Omega}\right)^{ee \rightarrow ee} \approx \left(\frac{d\sigma}{d\Omega}\right)_{\text{QED}}^{ee \rightarrow ee} + \frac{1}{M^2} \left\{ \frac{9}{4} \frac{\Gamma_{ee}^2}{\Gamma M} (1 + \cos^2 \theta) \left(1 + \frac{3}{4} \beta\right) \text{Im} f - \frac{3\alpha}{2} \frac{\Gamma_{ee}}{M} \left[ (1 + \cos^2 \theta) - \frac{(1 + \cos \theta)^2}{(1 - \cos \theta)} \right] \text{Re} f \right\}. \quad (26)$$

The first term represents the QED cross section calculated with the Monte Carlo technique [28, 29]. The second (resonance) and the third (interference) terms have been obtained in [20]. The corrections to the latter are not calculated precisely, but that does not limit the accuracy of the published results. Parameters  $\beta$  and  $f$  are defined by Eqs. (12) and (13), respectively.

## 6. Data analysis

### 6.1. Monte Carlo simulation

The simulation of the experiment was performed in the frame of the *GEANT* package, version 3.21 [30].

The  $\psi(2S)$  decays and the continuum multihadron events were generated with the tuned version of the BES generator [31] based on the JETSET 7.4 code [32]. At the original parameter settings of the BES generator the difference of the simulated charged multiplicity and that observed experimentally exceeds 1%, thus the bias in the detection efficiency up to 2% is expected. The procedure of the parameter tuning is discussed in detail below in Section 7.2. The decay tables were updated according to the recent PDG edition [24]. The results are presented in Fig. 2, where the most important event characteristics obtained in the experiment are compared with those in simulation. Good agreement is observed.

The detection efficiency for  $\tau^+\tau^-$  events was obtained using the KORALB event generator [33]. Bhabha events required for the precise luminosity determination were simulated using the BHWIDE generator [28].

### 6.2. Trigger efficiency and event selection

To reduce systematic errors due to trigger instabilities and uncertainties in the hardware thresholds, both experimental and simulated events pass through the software event filter during the offline analysis. It recalculates the PT and ST decisions with tighter conditions using a digitized response of the detector subsystems. To suppress the machine background to an acceptable level, the following PT conditions were used by OR:

- signals from  $\geq 2$  barrel scintillation counters,
- signal from the LKr calorimeter in the scan of 2006,
- coinciding signals of two CsI endcaps.

Signals from two particles with the angular separation  $\gtrsim 20$  degrees satisfy the ST conditions which are rather complicated. The MC simulation yields the trigger efficiency of about 0.96 for  $\psi(2S)$  decays. Because of a problem with electronics, the LKr calorimeter was not used in the analysis of 2004 data and that decreased the trigger efficiency to 0.91.

The performance of the detector subsystems and the machine background conditions were very different in 2004 and 2006, so that the selection criteria are also different.

2004 data, first and second scans:

- $\geq 3$  charged tracks,
- $\geq 2$  charged tracks from a common vertex in the interaction region ( $\rho < 7$  mm,  $|z| < 130$  mm),

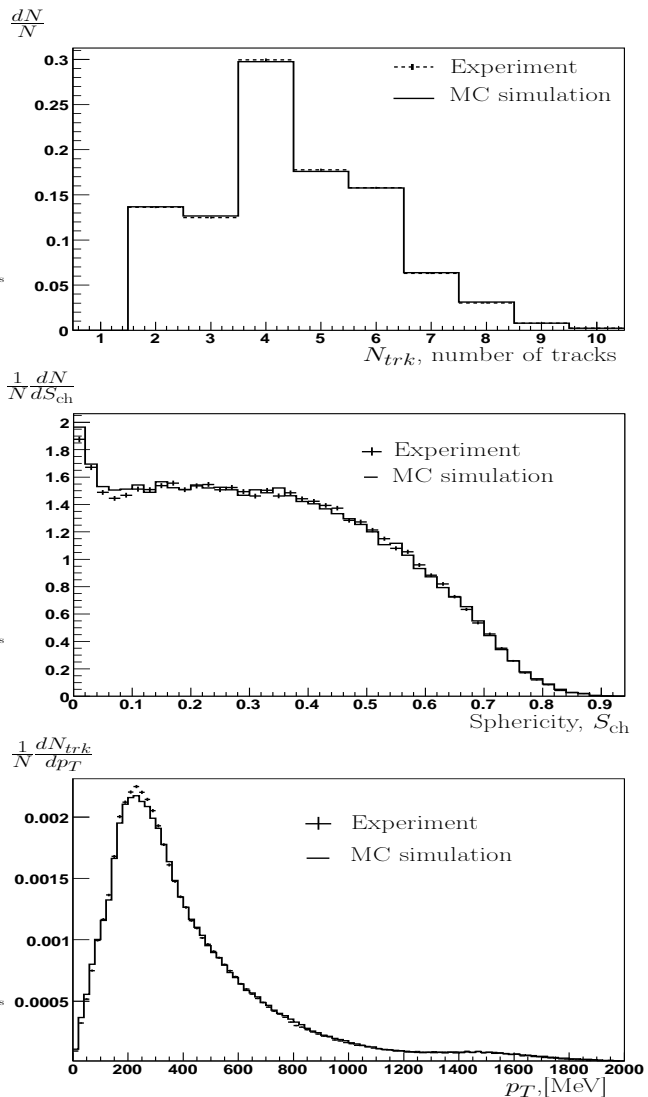


Figure 2: Properties of hadronic events produced in  $\psi(2S)$  decay. Here  $N$  is the number of events and  $p_T$  is the transverse momentum of a charged track. All distributions are normalized to unity.

- event sphericity  $S_{ch} > 0.05$ .

Here  $\rho$  and  $z$  are the track impact parameters relative to the beam axis and  $z$ -coordinate of the closest approach point.

The sphericity parameter is defined as

$$S = \frac{3}{2} \min \frac{\sum p_{T,i}^2}{\sum p_i^2}, \quad (27)$$

where summation is performed over all particles of the event and the minimum is taken over directions of the axis relative to which the transverse momenta  $p_{T,i}$  are calculated.  $S_{ch}$  is calculated using charged tracks only. The cut on  $S_{ch}$  is efficient for suppression of the  $e^+e^- \rightarrow e^+e^-\gamma$  background, that of cosmic rays and some kinds of the machine background, though it also suppresses the leptonic modes of the cascade decay  $\psi(2S) \rightarrow J/\psi + neutrals$  (see the low sphericity peak in Fig. 2).

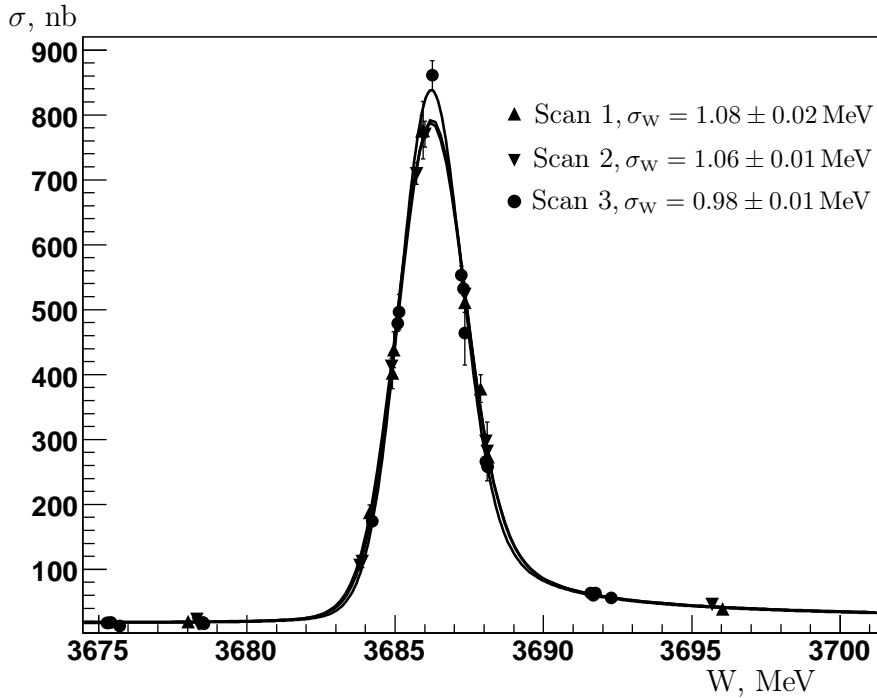


Figure 3: The multihadron cross section as a function of the c.m. energy for three scans. The curves are the results of the fits. All data are corrected for the efficiency, the peak cross section depends on the energy spread  $\sigma_W$ .

2006 data, third scan:

- $\geq 3$  charged tracks or two tracks with the acollinearity  $> 35$  degrees,
- $\geq 2$  charged tracks from a common vertex in the interaction region ( $\rho < 7$  mm,  $|z| < 130$  mm),
- $\geq 1$  photons with energy  $\geq 100$  MeV in the calorimeter,
- event sphericity  $S_{ch} > 0.05$ .
- the energy deposited in the calorimeter  $\geq 450$  MeV.

Analyzing the third scan we also used the alternative selection criteria without a tight cut on the sphericity, but with additional requirements on the calorimeter response. It allows us to check the systematic error due to the sphericity cut.

For additional suppression of the background induced by cosmic rays a veto from the muon system was required in the cases when more than two tracks did not cross the interaction region or the event arrival time determined by TOF relative to the bunch crossing was less than  $-5$  ns or larger than  $10$  ns. This condition was common for all three scans.

The conditions described above reduce the physical background contributions which do not scale with energy like  $1/s$  to a negligible level, except the tau pair production which we took into account explicitly in the observed cross section. The contribution of the beam-wall and beam-gas events, cosmic events and their coincidences was evaluated using data collected with the separated beams (about 10% of the full data sample). It was about 2% of the observed continuum cross section for the

third scan and about 0.4% for the first two. The analysis of the event vertex distribution along the beam axis confirmed these estimates. We did not perform the background subtraction in each data point as was done in the work [27] for precise  $R$  measurements. This is not required for the resonance parameter determination, the corresponding uncertainties are discussed in Section 7.3. Simulation of  $\psi(2S)$  decays yields the detection efficiencies of 0.63 and 0.72 for the two sets of selection criteria, respectively. To ensure the detection efficiency stability, all electronic channels malfunctioning in some runs during a scan were excluded from the analysis of all its runs.

### 6.3. Luminosity determination

The stability and absolute calibration accuracy of the bremsstrahlung monitors used for on-line luminosity measurements (Section 2) are not sufficient for the precision cross section analysis, thus events of Bhabha scattering were employed for the off-line luminosity determination. In 2004 it was provided by the endcap CsI calorimeter (the fiducial region  $20^\circ < \theta < 32^\circ$  and  $148^\circ < \theta < 160^\circ$ ). In the analysis of the 2006 data the LKr calorimeter was employed ( $40^\circ < \theta < 140^\circ$ ) while the CsI one served for cross-checks only.

The criteria for  $e^+e^-$  event selection using the calorimeter data are listed below:

- Two clusters with the energy above 0.25 of the beam energy and the angle between them exceeding 165 degrees,
- The total energy of these two clusters exceeds 1.05 times the beam energy,

- The calorimeter energy not associated with these two clusters does not exceed 10% of the total.

The loose energy cuts were chosen to reduce the influence of the calorimeter channels excluded from the analysis as was mentioned above. The tracking system was used only to reject the background ( $e^+e^- \rightarrow \gamma\gamma$  and  $e^+e^- \rightarrow \text{hadrons}$ ). The number of extra photons was required to be less than two for the additional suppression of the latter.

#### 6.4. Fitting procedure

The collision energy  $W$  was assigned to each data acquisition run using the interpolated results of the beam energy measurements and assuming  $W = 2E_{beam}$ . The runs with close  $W$  values were joined into points with the luminosity-weighted values  $W_i$  ( $i$  is the point number).

The numbers of hadronic events  $N_i$  and events of Bhabha scattering  $n_i$  observed at the  $i$ -th energy point were fitted as a function of  $W$  using the maximum likelihood method with a likelihood function

$$-2 \ln \mathcal{L} = 2 \sum_i \left[ N_i^{\text{obs}} \ln \left( \frac{N_i^{\text{obs}}}{N_i^{\text{exp}}} \right) + N_i^{\text{exp}} - N_i^{\text{obs}} + n_i^{\text{obs}} \ln \left( \frac{n_i^{\text{obs}}}{n_i^{\text{exp}}} \right) + n_i^{\text{exp}} - n_i^{\text{obs}} \right], \quad (28)$$

where  $N_i^{\text{exp(obs)}}$  and  $n_i^{\text{exp(obs)}}$  are the expected (observed) numbers of the hadronic and Bhabha events, respectively. The expected numbers of the hadronic and Bhabha scattering events were determined as follows:

$$\begin{aligned} N_i^{\text{exp}} &= \sigma_{\text{hadr}}(W_i) \cdot L_i, \\ n_i^{\text{exp}} &= \sigma_{e^+e^-}(W_i) \cdot L_i, \end{aligned} \quad (29)$$

here  $\sigma_{\text{hadr}}$  and  $\sigma_{e^+e^-}$  are defined by

$$\begin{aligned} \sigma_{\text{hadr}} &= \sigma_{\psi(2S)}^{\text{obs}}(W_i) + \varepsilon_{e^+e^-(\text{hadr})} \sigma_{e^+e^-}^{\text{obs}}(W_i), \\ \sigma_{e^+e^-} &= \sigma_{e^+e^-}^{\text{obs}}(W_i) + \varepsilon_{\text{hadr}(e^+e^-)} \sigma_{\psi(2S)}^{\text{obs}}(W_i), \end{aligned} \quad (30)$$

where  $\sigma_{\psi(2S)}^{\text{obs}}(W_i)$  and  $\sigma_{e^+e^-}^{\text{obs}}(W_i)$  were calculated according to (21) and by integration of (26), respectively. The detection efficiencies entering the formulae were determined separately at each point using the run-dependent Monte Carlo simulation. The values of the cross-feed selection efficiency  $\varepsilon_{e^+e^-(\text{hadr})}$  (the probability to select the  $e^+e^- \rightarrow e^+e^-$  event as the hadronic one) obtained by MC are about 0.006%, 0.006% and 0.37% for three scans, respectively. The corresponding values of  $\varepsilon_{\text{hadr}(e^+e^-)}$  are 0.03%, 0.03% and 0.25%.

The integrated luminosity  $L_i$  at the energy point  $i$  can be derived from the condition  $\partial/\partial L_i \ln \mathcal{L} = 0$ , giving

$$L_i = \frac{N_i^{\text{obs}} + n_i^{\text{obs}}}{\sigma_{\text{hadr}} + \sigma_{e^+e^-}}. \quad (31)$$

Using the likelihood function that takes into account both  $N_i$  and  $n_i$  ensures a correct estimation of the statistical uncertainty in the fit results.

Table 1: The main results of the scan fits (statistical errors only are presented).

	$M$ , MeV	$\Gamma_{ee} \times \mathcal{B}_h$ , keV	$P(\chi^2)$ , %
Scan 1	$3686.102 \pm 0.018$	$2.258 \pm 0.033$	15.8
Scan 2	$3686.130 \pm 0.013$	$2.229 \pm 0.024$	29.5
Scan 3	$3686.108 \pm 0.010$	$2.226 \pm 0.022$	79.5

The data of each scan were fitted separately, the free parameters were the  $\psi(2S)$  mass  $M$ ,  $\Gamma_{ee} \times \mathcal{B}_h$ , the energy spread  $\sigma_W$  and the continuum cross section magnitude  $\sigma_0$ . The  $\lambda$  parameter was fixed at the value of 0.13 according to Eq.(22). The data points ( $\sigma_i, W_i$ ) and the fitted curves are shown in Fig. 3. The results of the fits are presented in Table 1.

The statistical accuracy of the mass values is significantly better than that for the three scans performed at VEPP-4M in 2002 [10]. The combined analysis is required to take into account properly the systematic errors of the six mass values. It will be described in a separate paper discussing numerous accelerator-related effects. For this reason we omit such a discussion below and just present the result and error estimates. The analysis of the three values obtained in this work gives

$$M = 3686.114 \pm 0.007 \pm 0.011^{+0.002}_{-0.012} \text{ MeV.}$$

The model dependence of the mass value was estimated floating the  $\lambda$  parameter in the fit.

## 7. Discussion of systematic uncertainties in $\Gamma_{ee} \times \mathcal{B}_h$

The dominating sources of the systematic uncertainty in the  $\Gamma_{ee} \times \tilde{\mathcal{B}}_h = \Gamma_{ee} \times \tilde{\Gamma}_h/\Gamma$  value are discussed in the following subsections. The issue of the difference between  $\tilde{\Gamma}_h$  and the sum of hadronic partial widths because of possible correlations of interference phases is addressed in the next section.

### 7.1. Systematic error of absolute luminosity determination

The major contributions to the uncertainty of the absolute luminosity determination are presented in Table 2.

Table 2: Systematic uncertainties of the luminosity determination in % for three scans. The correlated parts of the uncertainties are also presented. The uncertainties for the first and second scans are assumed to be fully correlated.

Source	Scan 1	Scan 2	Scan 3	Common
Calorimeter calibration	0.3	0.3	0.7	0.2
Calorimeter alignment	0.3	0.3	0.1	0.1
Polar angle resolution	0.8	0.8	0.2	-
Cross section calculation	0.5	0.5	0.5	0.4
Background	0.1	0.1	0.1	0.1
MC statistics	0.1	0.1	0.1	-
Variation of cuts	<1.3	<1.4	<0.9	<0.2
<i>Sum in quadrature</i>	$\approx 1.6$	$\approx 1.7$	$\approx 1.2$	$\approx 0.5$

The uncertainty due to the calorimeter energy calibration was estimated by variation of simulation parameters concerning the GEANT performance, the light yield uniformity in CsI crystals, a sensitivity to the energy loss fluctuations between LKr calorimeter electrodes etc. Additionally, the CsI individual channel calibrations using cosmic rays and Bhabha events were compared.

The LKr calorimeter was aligned with respect to the drift chamber using cosmic tracks reconstructed in the DC. Then eight modules of the CsI calorimeters were aligned relative to the LKr calorimeter using cosmic rays reconstructed in the LKr strip system. The beam line position and direction were determined using the primary vertex distribution of multihadron events. The inaccuracy of the alignment resulted in the error of the luminosity measurements of about 0.3% for CsI and about 0.1% for LKr.

The difference in the polar angle resolutions observed experimentally and predicted by MC causes an uncertainty in the luminosity measurement, since events migrate into or out of the fiducial volume. These errors are 0.8% and 0.2% for the CsI and LKr calorimeters, respectively.

The uncertainty of the theoretical Bhabha cross section was estimated comparing the results obtained with the BHWIDE [28] and MCGPJ [29] event generators. It agrees with the errors quoted by the authors. The value of 0.5% quoted in Table 2 includes also the accuracy of Eq. (26).

The background to the Bhabha process from the  $\psi(2S)$  decays and reactions  $e^+e^- \rightarrow \mu\mu(\gamma)$  and  $e^+e^- \rightarrow \gamma\gamma$  was estimated using MC simulation. It contributes less than 0.3% to the luminosity. The resonant part of the background contribution was taken into account in the fit (Section 6.4). The residual luminosity uncertainty due to background does not exceed 0.1%.

In order to estimate the effect of other possible sources of uncertainty, the variation of the cuts was performed within the fiducial region in which good agreement between the MC simulation and experiment is observed. The cut on the deposited energy was varied in the range of 55 – 75% of the c.m. energy. The cuts on the polar angle were varied in a range much larger than the angular resolution, the variation in the Bhabha event count reaches 40%. The variations discussed above correspond to a systematic uncertainty shown in Table 2. These effects can originate from the already considered sources and statistical fluctuations, nevertheless we included them in the total uncertainty to obtain conservative error estimates.

Finally, we compared an integrated luminosity obtained using the LKr and CsI calorimeters in the scan of 2006. The difference of about  $1.1 \pm 1.0\%$  was found which is consistent with the estimates in Table 2.

## 7.2. Uncertainty due to imperfect simulation of $\psi(2S)$ decays

The imperfect simulation of  $\psi(2S)$  decays contributes significantly to the  $\Gamma_{ee} \times \mathcal{B}_h$  systematic error caused by the detection efficiency uncertainty. Eventually, this uncertainty is determined by the experimental statistics available for the event generator tuning and the ability of the latter to reproduce distributions of parameters essential for the event selection and

their correlations. In our case such parameters are the charged multiplicity and event sphericity calculated using momenta of charged tracks.

The selection criteria described in Section 6.2 reject low-multiplicity events. The corresponding branching fractions are either negligible like for  $\psi(2S) \rightarrow \pi^+\pi^-$  or well measured like for  $\psi(2S) \rightarrow J/\psi \eta \rightarrow \mu^+\mu^-\gamma\gamma$ . Such decays are simulated in the BES generator [31] explicitly. The variation of decay table parameters within their errors (Ref. [24]) indicates the detection efficiency uncertainty of less than or about 0.3%. The dominating uncertainty comes from decays of higher multiplicity which are simulated using the parton approach and the fragmentation model incorporated in the JETSET 7.4 code.

About 60% of the  $\psi(2S)$  decays include  $J/\psi$  which is at the edge or even beyond the region where the JETSET results can be trusted, nevertheless it has enough options and parameters to achieve good agreement with experiment for major event characteristics (Fig. 2) and to estimate the detection efficiency uncertainty. To do this we iterated as follows:

1. select a critical option or parameter and modify it using an educated guess;
2. select a complementary parameter and modify it to find the value at which the observed charged multiplicity agrees with experiment;
3. calculate the detection efficiency and compare it with previous results to estimate the uncertainty.

In addition to the charged multiplicity, the observed distributions in the sphericity parameter, the invariant mass of the pairs of the opposite signs and the inclusive momentum spectrum were controlled. The versions of the simulation obviously contradicting to experiment were rejected. The results are presented in Table 3 and illustrated by Fig. 4.

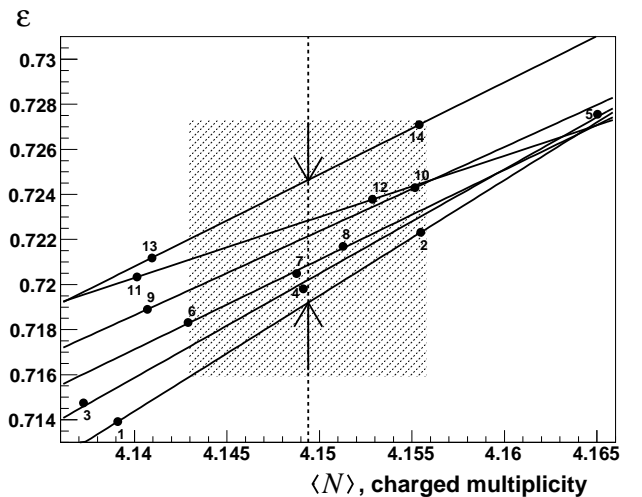


Figure 4: Detection efficiency vs. charged multiplicity for different versions of the  $\psi(2S)$  decay simulation. The fit lines correspond to variation of one of the selected parameters. The shadow box corresponds to the statistical error of the charged multiplicity. The statistical error of the efficiency  $\sim 0.001$  is not shown.

The following JETSET options were studied:

Table 3: Comparison of different versions of the MC simulation of  $\psi(2S)$  decays.

Version	JETSET modifications		Charged multiplicity	Efficiency, %	
<b>LUND fragmentation function</b>					
<i>Probability of vector meson formation</i>					
	$P_V$	$\sigma_{p_T}$ , GeV			
1	0.50	0.55	$4.1391 \pm 0.0031$	$71.392 \pm 0.090$	
2	0.50	0.65	$4.1555 \pm 0.0031$	$72.232 \pm 0.090$	
<i><math>W_{\text{stop}}, W_{\text{min}}, \sigma_{p_T}</math> varied</i>					
	$W_{\text{stop}}$ , GeV	$W_{\text{min}}$ GeV	$\sigma_{p_T}$ , GeV		
6	0.47	0.8	0.65	$4.1429 \pm 0.0031$	$71.783 \pm 0.090$
7	0.52	0.8	0.65	$4.1488 \pm 0.0031$	$72.049 \pm 0.090$
8	0.56	0.8	0.65	$4.1512 \pm 0.0031$	$72.170 \pm 0.090$
<i><math>\delta W_{\text{stop}}, \sigma_{p_T}</math> varied</i>					
	$\delta W_{\text{stop}}$	$\sigma_{p_T}$ , GeV			
9	0.17	0.7	$4.1407 \pm 0.0031$	$71.890 \pm 0.090$	
10	0.17	0.65	$4.1552 \pm 0.0031$	$72.430 \pm 0.090$	
<i><math>W_{\text{min}}, \sigma_{p_T}</math> varied</i>					
	$W_{\text{min}}$ , GeV	$\sigma_{p_T}$ , GeV			
11	0.8	0.675	$4.1401 \pm 0.0031$	$72.033 \pm 0.090$	
12	0.8	0.65	$4.1529 \pm 0.0031$	$72.378 \pm 0.090$	
<b>Switched off parton shower</b>					
	$\sigma_{p_T}$ , GeV				
13	0.65		$4.1409 \pm 0.0031$	$72.118 \pm 0.090$	
14	0.55		$4.1554 \pm 0.0031$	$72.709 \pm 0.090$	
<b>Field-Feynman fragmentation function</b>					
	$W_{\text{stop}}$ , GeV	$\sigma_{p_T}$ , GeV			
3	0.62	0.58	$4.1372 \pm 0.0031$	$71.475 \pm 0.090$	
4	0.62	0.50	$4.1491 \pm 0.0031$	$71.981 \pm 0.090$	
5	0.62	0.43	$4.1650 \pm 0.0031$	$72.755 \pm 0.090$	

1. LUND fragmentation function, parton showers are on;
2. LUND fragmentation function, parton showers are off;
3. Field-Feynman fragmentation function, parton showers are on;
4. independent fragmentation, all momentum conservation options.

No acceptable versions were obtained in the latter case. For the LUND fragmentation function the influence of a few most critical parameters was investigated.

The main parameters controlling the fragmentation process in JETSET are PARJ(32), PARJ(33) and PARJ(37) (we refer to them as  $W_{\text{min}}$ ,  $W_{\text{stop}}$  and  $\delta W_{\text{stop}}$ , respectively, in Table 3 and below). The fragmentation of a colour-singlet system formed by initial partons or during the parton showering proceeds while the energy is greater than  $W_{\text{min}}$  plus quark masses, otherwise a pair of hadrons is to be produced. The  $W_{\text{stop}}$  parameter serves to terminate the fragmentation and produce a final hadron pair earlier, taking into account the mass of the last quark pair produced. To avoid artifacts in the hadron momentum spectrum, the stopping point energy is smeared using the  $\delta W_{\text{stop}}$  parameter (20% by default). The transverse momentum of quarks appearing during the fragmentation is controlled by the parameter

PARJ(21) ( $\sigma_{p_T}$ ). The parameter PARJ(11) ( $P_V$ ) determines the probability that a light meson formed in the fragmentation has spin 1. The default values of the parameters  $W_{\text{min}}$ ,  $W_{\text{stop}}$ ,  $\sigma_{p_T}$  and  $P_V$  in JETSET are 1., 0.8, 0.36 GeV and 0.5, respectively. The corresponding values set in the BES generator are 1., 0.6, 0.5 GeV and 0.6.

Figure 4 shows the values of the detection efficiency and observed charged multiplicity for the sets of options and parameters listed in Table 3. The dashed line corresponds to the charged multiplicity observed in experiment with the selection criteria of the 2006 scan,  $\langle N_{\text{exp.}} \rangle = 4.1494 \pm 0.0054$ . The maximum difference between the detection efficiency values at the point of the multiplicity agreement is 0.55% with the central value of about 72.19%. This is presented with the segment between the arrows and its middle point in Fig. 4. The experimental and simulated multiplicities have statistical errors, therefore the segment of the agreement transforms to the rectangle shown with the shadow box. Taking its angles we found the confidence interval of  $(72.16 \pm 0.57)\%$  and from that derived that the relative uncertainty of the detection efficiency due to ambiguity in the choice of the JETSET parameter set is about 0.8%. A very similar central value of 72.11% was obtained by averaging the fourteen efficiencies from Table 3 with the weights inversely

proportional to the sum of  $\chi^2$  for the four event characteristics under control.

There is a systematic error in the observed multiplicity related to the track reconstruction efficiency, which is not exactly the same for the experimental data and simulation. The difference was studied using Bhabha events and low-momentum cosmic tracks and the appropriate correction was introduced in the detector simulation. However, the inaccuracy of the correction increases the shadow box size in Fig. 4 thus increasing the detection efficiency uncertainty. For the first two scans the effect is about 0.4% and it grows up to 0.7% for the third scan because of some problems in the drift chamber.

We repeated the procedure described above with the alternative set of event selection criteria and obtained a slightly different uncertainty estimate. To account for this we introduced an additional error of 0.3%.

The contributions to the detection efficiency uncertainty due to imperfect simulation of  $\psi(2S)$  decays are summarized in Table 4.

### 7.3. Detector- and accelerator-related uncertainties in $\Gamma_{ee} \times \mathcal{B}_h$

The major sources of the systematic uncertainty in the  $\Gamma_{ee} \times \mathcal{B}_h$  product are listed in Table 5.

The systematic error related to the efficiency of the track reconstruction was considered in the previous section. The trigger efficiency uncertainty is mainly due to the uncertainty of the calorimeter thresholds in the secondary trigger. The estimate of about 0.2% was obtained varying the threshold in the software event filter. The excess of the filter threshold over the hardware one in units of the hardware threshold width was varied from 5 to 6.

The trigger efficiency for all scans and the event selection efficiency for the third one depend on the calorimeter response to hadrons. Their nuclear interaction was simulated employing the GEISHA [35] and FLUKA [36] packages as they are implemented in GEANT 3.21 [30]. Both of them satisfactorily reproduce the pion signal in CsI, but in liquid krypton the performance of GEISHA is much better, thus we determined the efficiencies using it and estimated the systematic errors comparing the results obtained with two packages.

The crosstalks in the vertex detector electronics introduced a variation of the detection efficiency up to 1.5% because of the cut on the total number of VD hits in the on-line event selection software (Section 2). A code simulating the crosstalks was developed and tuned using either events of Bhabha scattering or cosmic rays. The residual uncertainty thus determined is about  $0.1 \div 0.2\%$  depending on the VD voltage.

The effect of other possible sources of the detector-related uncertainty was evaluated by varying the event selection cuts. The conditions on the number of tracks were tightened one by one for all three scans. For the last one a cut on the energy deposited in the calorimeter was also increased by the most probable photon energy. The detection efficiency varied from 0.53 to 0.63 in the 2004 scans and from 0.70 to 0.79 in the 2006 scan. The maximum variations of the  $\Gamma_{ee} \times \mathcal{B}_h$  result are presented in Table 5.

The systematic error in the  $\Gamma_{ee} \times \mathcal{B}_h$  value due to the beam energy determination (Ref. [7]) and the data point formation (Section 6.4) was studied for each scan. The relative error does not exceed 0.2% except the third scan which includes one point with a significant accelerator instability that increases the error up to 0.6%.

The non-Gaussian effects in the total collision energy distribution contribute about 0.2% to the  $\Gamma_{ee} \times \mathcal{B}_h$  uncertainty. Changing the zero value of the  $a$  parameter entering the pre-exponential factor (24) to the value measured with the specific accelerator technique leads to the mass shift of a few keV [10] and causes a negligible bias in the  $\Gamma_{ee} \times \mathcal{B}_h$  value which is related to the area under the resonance excitation curve. The quoted estimate was obtained by releasing the  $b$  parameter.

The bias in the resonance parameters due to the admixture of the machine and cosmic background to selected multihadron events was evaluated with the controllable increase of this admixture. For each data point the background event sample was formed containing the events which passed some loose selection criteria but were rejected by the multihadron ones. The number of multihadrons events was increased by such fraction of the background sample size, that the data fit yielded 2% (0.4%) growth of the continuum cross section for the third (first and second) scan in accordance with the background estimates quoted in Section 6.2. The variation of the  $\psi(2S)$  mass value did not exceed 1 keV, the change of the  $\Gamma_{ee} \times \mathcal{B}_h$  product was less than 0.1%.

### 7.4. Other uncertainties

In this subsection we discuss the uncertainties related to the iterations used to obtain the total and electron width values (Section 5), the fixation of the interference parameter  $\lambda$  entering the multihadron cross section (10), and the accuracy of the theoretic formulae employed for the calculation of the cross section. Using various initial values for the total and electron width we have verified that the iteration procedure converges fast introducing a negligible systematic uncertainty. To reduce the statistical error on the  $\psi(2S)$  mass, the interference parameter  $\lambda$  was fixed in the fit at the value of 0.13 corresponding to Eq. (22). Releasing the  $\lambda$  parameter in the fit shifts the  $\Gamma_{ee} \times \mathcal{B}_h$  value by -0.23%. This quantity can be used as an estimate of the influence of quasi-two-body decays with correlated interference phases mentioned in Section 5.2. The accuracy of the resonance term in Eq. (10) is about 0.1% (Section 5), and another 0.1% should be added because of the accuracy of radiative correction calculations in Ref. [15]. The quadratic sum of these three contributions is about 0.3%.

## 8. Inaccuracy due to interference in hadronic cross section

The fits done with a floating interference parameter gave

$$\lambda = 0.21 \pm 0.07 \pm 0.05$$

The systematic uncertainty is mainly due to the beam energy determination and stability of the cross section measurement.

Table 4: Systematic uncertainties of the detection efficiency due to  $\psi(2S)$  decay simulation in % for three scans. The correlated parts of the uncertainties are also presented. The uncertainties for the first and second scans are assumed to be fully correlated.

<i>Source</i>	Scan 1	Scan 2	Scan 3	Common
Measured branchings	0.4	0.4	0.3	0.3
JETSET ambiguities	0.8	0.8	0.8	0.8
Track reconstruction	0.4	0.4	0.7	0.4
Selection criteria	0.3	0.3	0.3	0.3
MC statistics	0.1	0.1	0.1	-
<i>Sum in quadrature</i>	$\approx 1.0$	$\approx 1.0$	$\approx 1.1$	$\approx 1.0$

Table 5: The dominating systematic uncertainties in the  $\Gamma_{ee} \times \mathcal{B}_h$  product for three scans (%). The correlated parts of the uncertainties are also presented. The inaccuracy of about 0.9% due to possible interference phase correlation is not included.

<i>Source</i>	Scan 1	Scan 2	Scan 3	Common <sub>12</sub>	Common <sub>123</sub>
Absolute luminosity measurements	1.6	1.7	1.2	1.6	0.5
$\psi(2S)$ decay simulation	1.0	1.0	1.1	1.0	1.0
Detector response					
Trigger efficiency	0.2	0.2	0.2	0.2	0.2
Nuclear interaction	0.2	0.2	0.3	0.2	0.2
Cross talks in VD	0.1	0.17	0.1	0.1	0.1
Variation of cuts	0.5	0.3	0.6	0.3	0.3
Accelerator related effects					
Beam energy determination	0.15	0.18	0.6	0.15	0.15
Non-Gaussian energy distribution	0.2	0.2	0.2	0.2	0.2
Residual background	<0.1	<0.1	<0.1	<0.1	<0.1
Other uncertainties	0.3	0.3	0.3	0.3	0.3
<i>Sum in quadrature</i>	$\approx 2.0$	$\approx 2.1$	$\approx 1.9$	$\approx 2.0$	$\approx 1.3$

This result does not contradict to the assumption of the uncorrelated interference phases (Section 5.2) but can still indicate the presence of some phase correlations.

In order to evaluate a possible deviation of the  $\tilde{\Gamma}_h$  value from the sum of hadronic partial widths  $\Gamma_h$ , we performed a Monte Carlo simulation according to Eq. (18) and (19). The set of decay modes and the corresponding branching fractions were obtained using the event generator described in Section 6.1, with the number of different decay modes exceeding one thousand. Damping of  $\sin \phi_m$  and  $\cos \phi_m$  because of the averaging  $\langle \rangle_{\Theta}$  was ignored.

The inaccuracy in  $\Gamma_h$  was estimated in the Bayesian approach. Possible sets of interference phases  $\phi_m$  are characterized by the central value  $\phi$  and the band width  $\Delta\phi$ . It was assumed that probabilities of all  $\phi$  and  $\Delta\phi$  values are equal. The result is not sensitive to assumptions on the band shape.

The Monte Carlo procedure consists of two steps. At the first step in each Monte Carlo sampling a set of  $\phi_m$  was generated for random  $\phi$  and  $\Delta\phi$  and the corresponding  $\lambda$  value was calculated. The values of  $\phi$ ,  $\Delta\phi$  and  $\lambda$  were saved for the second step. The first-step distribution in  $\lambda$  is symmetric relative to the most probable value of 0.13 corresponding to Eq. (14). At the second step an acceptance-rejection (Von Neumann's) method

was employed to reproduce the  $\lambda$  distribution matching the results of the measurement: the Gaussian with the average value of 0.21 and the width of 0.086. The second-step distribution in  $(\tilde{\Gamma}_h - \Gamma_h)/\Gamma_h$  is peaked at zero. It is not Gaussian but 68% percent of the accepted samplings are contained in the interval of  $\pm 0.009$ , thus we concluded that the inaccuracy due to possible interference phase correlations in  $\Gamma_{ee} \times \mathcal{B}_h$  value is about 0.9%. Since the Bayesian approach was employed, appearance of the new information on the interference in the hadronic cross section can change this estimate.

It should be noted that the inaccuracy estimated in this section is not specific for our results on the  $\psi(2S)$  partial and total widths but is shared by many results obtained in other experiments using the  $\psi(2S)$  multihadron cross section. The most precise of them is the result of CLEO on the  $\psi(2S) \rightarrow J/\psi \pi^+ \pi^-$  branching fraction [37], its quoted accuracy is 2.2%. That concerns, in particular, the works [2, 3].

## 9. Averaging of scan results

The systematic errors on the  $\Gamma_{ee} \times \mathcal{B}_h$  values for three scans and the estimates of their correlations are presented in Table 5. The correlation of errors is a difficult issue. In non-obvious

cases the most conservative approach was used assuming that the correlated part corresponds to the minimal uncertainty in scans for a given uncertainty source.

To obtain the resulting value of the  $\Gamma_{ee} \times \mathcal{B}_h$  product, the scans were treated as independent experiments. The individual  $\Gamma_{ee} \times \mathcal{B}_h$  values were weighted using their statistical errors and uncorrelated parts of systematic errors. Such procedure takes into account the random behaviour of uncorrelated systematic errors thus converting them to statistical. Correspondingly, the systematic errors of individual scans reduce to their common part. The formal weighting recipe for the parameter  $\Gamma_{ee} \times \mathcal{B}_h$  is given below:

$$\begin{aligned} \langle \Gamma_{ee} \times \mathcal{B}_h \rangle &= \sum w_i \cdot (\Gamma_{ee} \times \mathcal{B}_h)_i, \\ \sigma_{\text{stat}}^2 &= \sum w_i^2 \cdot \sigma_{\text{stat},i}^2, \\ \sigma_{\text{syst}}^2 &= \sum w_i^2 \cdot (\sigma_{\text{syst},i}^2 - \sigma_{\text{syst},0}^2) + \sigma_{\text{syst},0}^2, \\ w_i &= 1 / (\sigma_{\text{stat},i}^2 + \sigma_{\text{syst},i}^2 - \sigma_{\text{syst},0}^2), \end{aligned} \quad (32)$$

where  $\sigma_{\text{syst},0}$  denotes a common part of systematic uncertainties. The recipe preserves the total error of the result.

## 10. Summary

The parameters of  $\psi(2S)$  have been measured using the data collected with the KEDR detector at the VEPP-4M  $e^+e^-$  collider in 2004 and 2006. Our final result for the  $\Gamma_{ee} \times \mathcal{B}_h$  product is

$$\Gamma_{ee} \times \mathcal{B}_h = 2.233 \pm 0.015 \pm 0.037 \pm 0.020 \text{ keV}.$$

The third error quoted is an estimate of the model dependence of the result due to assumptions on the interference effects in the cross section of the single-photon  $e^+e^-$  annihilation to hadrons explicitly considered in this work. Implicitly, the same assumptions were employed to obtain the charmonium leptonic width and the absolute branching fractions in many experiments. This quantity was measured in several experiments but only the result of MARK-I [38], an order of magnitude less precise than ours, was published in such a form. Usually the  $\Gamma_{ee} \times \mathcal{B}_h$  product is converted to the electron width value using existing results on the branching fraction to hadrons  $\mathcal{B}_h$  or the leptonic branching fractions.

Using the world average values of the electron and hadron branching fractions from PDG [24] we obtained the electron partial width and the total width of  $\psi(2S)$ :

$$\begin{aligned} \Gamma_{ee} &= 2.282 \pm 0.015 \pm 0.038 \pm 0.021 \text{ keV}, \\ \Gamma &= 296 \pm 2 \pm 8 \pm 3 \text{ keV}. \end{aligned}$$

These results are consistent with and more than two times more precise than any of the previous experiments.

The result on the  $\psi(2S)$  mass obtained in this work

$$M = 3686.114 \pm 0.007 \pm 0.011 \begin{matrix} +0.002 \\ -0.012 \end{matrix} \text{ MeV}.$$

The statistical uncertainty is significantly reduced compared to that reached at VEPP-4M in 2002, the systematic one is approximately the same. Since the systematic and model errors are correlated, the combined analysis of the 2002, 2004 and 2006 data has to be performed. It will be described in a dedicated paper the result of which should supersede the results presented above and in Ref. [10]. The reduction of the model dependence is expected.

## Acknowledgments

We greatly appreciate the efforts of our VEPP-4M colleagues to provide good operation of the accelerator complex and the staff of experimental laboratories for the permanent support in preparing and performing this experiment. The authors are grateful to V. P. Druzhinin, P. Wang and C. Z. Yuan for useful discussions and thank V. S. Fadin for a verification of results presented in Section 4.

The work is supported in part by the Ministry of Education and Science of the Russian Federation and grants Sci.School 6943.2010.2, RFBR 10-02-00695, 11-02-00112, 11-02-00558.

## References

- [1] N. Brambilla *et al.*, Eur. Phys. J. C **71** (2011) 1534.
- [2] J. Z. Bai *et al.* [BES Collaboration], Phys. Lett. B **550** (2002) 24.
- [3] M. Ablikim *et al.* [BES Collaboration], Phys. Rev. Lett. **97** (2006) 121801.
- [4] M. Ablikim *et al.* [BES Collaboration], Phys. Lett. B **660** (2008) 315.
- [5] M. Ablikim *et al.* [BES Collaboration], Phys. Lett. B **659** (2008) 74.
- [6] V. Anashin *et al.*, Stockholm 1998, EPAC 98\* (1998) 400, Prepared for 6th European Particle Accelerator Conference (EPAC 98), Stockholm, Sweden, 22-26 June 1998.
- [7] V. E. Blinov *et al.*, Nucl. Instr. and Meth. A **598** (2009) 23. Proc. of EPAC-2006 (2006).
- [8] A. D. Bukin *et al.*, Absolute Calibration of Beam Energy in the Storage Ring. Phi-Meson Mass Measurement, Preprint IYF-75-64, 1975.
- [9] A. N. Skrinsky and Y. M. Shatunov, Sov. Phys. Usp. **32** (1989) 548.
- [10] V. M. Aulchenko *et al.* [KEDR Collaboration], Phys. Lett. B **573** (2003) 63.
- [11] V. E. Blinov *et al.*, ICFA Beam Dyn. Newslett. **48** (2009) 195.
- [12] V. V. Anashin *et al.*, Nucl. Instrum. Meth. A **478** (2002) 420.
- [13] S. E. Baru *et al.*, Instrum. Exp. Tech. **54** (2011) 335.
- [14] A. G. Shamov [KEDR Collaboration], Chinese Phys. C **84** (2010) 836 Proc. of Int. Workshop on  $e^+e^-$  Collision from  $\phi$  to  $\psi$ , Beijing, 2009. arXiv: hep-ex/1110.0328.
- [15] E. A. Kuraev and V. S. Fadin, Sov. J. Nucl. Phys. **41** (1985) 466.
- [16] F. A. Berends, G. J. Komen, Nucl. Phys. B **115** (1976) 114.
- [17] H. Burkhardt *et al.*, Z. Phys. C **43** (1989) 497.
- [18] J. P. Alexander *et al.*, Nucl. Phys. B **320**, 45 (1989).
- [19] D. Zhang *et al.*, Phys. Rev. D **74** (2006) 054012
- [20] Y. I. Azimov *et al.*, JETP Lett. **21** (1975) 172.
- [21] K. Yu. Todyshev, arXiv:0902.4100.
- [22] R. N. Cahn, Phys. Rev. D **36** (1987) 2666, [Erratum-ibid. D **40** (1989) 922].
- [23] P. Wang *et al.*, Phys. Lett. B **593** (2004) 89.
- [24] K. Nakamura *et al.*, J. Phys. G **37** (2010) 075021.
- [25] M. Z. Yang, Mod. Phys. Lett. A **23** (2008) 3113
- [26] M. B. Voloshin, Phys. Lett. B **556** (2003) 153.
- [27] M. Ablikim *et al.* [BES Collaboration], Phys. Lett. B **677** (2009) 235.
- [28] S. J. Jadach, W. Placzek, B.F.L. Ward, Phys. Lett. B **390** (1997) 298.
- [29] A. B. Arbuzov *et al.*, Eur. Phys. J. C **46** (2006) 689.
- [30] GEANT – Detector Description and Simulation Tool CERN Program Library Long Writeup W5013.

- [31] J.C. Chen *et al.*, Phys. Rev. D **62** (2000) 034003.
- [32] T. Sjostrand, M. Bengtsson, Comp. Phys. Comm. **43** (1987) 367.
- [33] S. Jadach, Z. Was, Comp. Phys. Comm. **85** (1995) 453.
- [34] T. Sjostrand, S. Mrenna, P. Skands, PYTHIA 6.4 Physics and Manual, arXiv:hep-ph/0603175.
- [35] H.C. Fesefeldt, Technical Report PITHA-85-02, III Physikalisches Institut, RWTH Aachen Physikzentrum, 5100 Aachen, Germany, Sep. 1985.
- [36] A. Fassò *et al.*, Talk from the Computing in High Energy and Nuclear Physics (CHEP03), arXiv:physics/0306162.
- [37] H. Mendez *et al.* [CLEO Collaboration], Phys. Rev. D **78**, 011102 (2008).
- [38] G.S. Abrams, Symposium On Lepton and Photon Interactions At High Energies, Stanford 1975, 25.